Optical signatures of exciton polarons from diagrammatic Monte Carlo

A. S. Mishchenko,[1,2] G. De Filippis,[3] V. Cataudella,[3] N. Nagaosa,[1,4] and H. Fehske[5]
[1]*RIKEN Center for Emergent Matter Science (CEMS), 2-1 Hirosawa, Wako, Saitama 351-0198, Japan*
[2]*NRC "Kurchatov Institute", 123182 Moscow, Russia*
[3]*SPIN-CNR and Dept. of Physics, University of Napoli "Federico II" I-80126 Napoli, Italy*
[4]*Department of Applied Physics, The University of Tokyo, 7-3-1 Hongo, Bunkyo-ku, Tokyo 113, Japan*
[5]*Institut für Physik, Ernst-Moritz-Arndt-Universität Greifswald, 17489 Greifswald, Germany*

(Received 6 April 2017; revised manuscript received 5 January 2018; published 22 January 2018)

We study the interplay of electron-electron and electron-phonon interactions in the course of electron-hole bound-state formation for gapped solid-state systems. Adapting the essentially approximation-free diagrammatic Monte Carlo method for the calculation of the optical response, we discuss the absorption of light in correlated electron-phonon systems for the whole interaction and phonon frequency regimes. The spectral function obtained by analytical continuation from the imaginary-time current-current correlation function demonstrates the dressing of excitons by a phonon cloud when the coupling the lattice degrees of freedom becomes increasingly important, where notable differences show up between the adiabatic and antiadiabatic cases.

DOI: 10.1103/PhysRevB.97.045141

I. INTRODUCTION

Optical properties of semiconductors and insulators are connected with interband transitions between the highest occupied and lowest unoccupied bands, which can be probed by standard light absorption measurements [1,2]. On the theoretical side, a full many-particle treatment of the resulting electron-hole systems is difficult, in particular if the (excitation) gap originates from strong electronic correlations or coupling to the lattice degrees of freedom. The situation greatly simplifies in the low-excitation regime, where an extremely small density of electrons and holes exists, and one can concentrate on the analysis of electron-hole pairing effects. Here the Coulomb interaction between conduction-band electrons and valence-band holes mainly triggers the formation of in-gap excitonic bound states in various materials ranging from one-dimensional (1D) to three-dimensional (3D) ones [3–7]. Since the electron-hole pairs are electrically neutral and the coupling between carriers and optical phonons in polar compounds is electrical in nature, one naively would expect that the exciton-phonon interaction is weak. However, the coupling of carriers to phonons in nonpolar solids is governed by deformation potential. It was clear from the initial concept [8] and then confirmed by numerous studies, e.g., [9,10], that there is no fixed relation between the signs of the deformation potentials of valence and conduction bands. Thus, the exciton-phonon interaction can be significant.

One prominent example is robust exciton polarons in (quasi-zero-dimensional) semiconductor quantum dots which strongly modify the photoluminescence (optical response) because the exciton and phonon states are entangled [11,12]. Phonon-assisted electron-hole bound-state formation also quite often takes place in quasi-one-dimensional solids, such as polydiacethylene crystals [13]. Particularly fascinating, the lattice seems to be involved in the phase transition to an excitonic insulator state which recently has been discussed for a number of interesting materials at large exciton densities [14–17]. For example, in semiconducting Ta_2NiSe_5, the lattice structure changes from orthorhombic to monoclinic at the suggested excitonic instability [18]. A combination of excitonic and lattice instabilities has been made responsible for the observed (possibly chiral) charge-density wave in the layered transition-metal dichalcogenide $1T-TiSe_2$ [19]. Finally, in the intermediate-valent $TmSe_{0.45}Te_{0.55}$ compound the (thermo)transport seems to be indicative of exciton polarons as well [20,21].

Attempts to tackle theoretically the underlying tricky exciton-polaron formation problem consider the exciton as a preformed structureless quasiparticle object [22,23]. In addition, the frozen-phonon approximation was frequently used [4], or simple variational approaches were exploited [24]. The recently developed diagrammatic Monte Carlo (DMC) technique [25–27] seems to be especially suitable to address the long-standing exciton-polaron issue more seriously [28]. Therefore, in the present paper, we generalize and apply the DMC to the calculation of light absorption by a coupled electron-hole-lattice system described by a generic microscopic model. In this way we are able to provide exact numerical results for the optical response in the whole parameter range of Coulomb interaction, fermion-phonon coupling, and phonon frequency.

II. MODELING APPROACH

A. Exciton-polaron Hamiltonian

The two-band model under consideration is

$$H = \sum_{\mathbf{k}} \varepsilon_c(\mathbf{k})\, e^\dagger_{\mathbf{k}} e_{\mathbf{k}} + \sum_{\mathbf{k}} \varepsilon_v(\mathbf{k})\, h_{\mathbf{k}}\, h^\dagger_{\mathbf{k}} + \sum_{\mathbf{q}} \omega_{\mathbf{q}}\, b^\dagger_{\mathbf{q}} b_{\mathbf{q}} - \sum_{\mathbf{kq}} \left[\frac{g_e(\mathbf{q})}{\sqrt{N}} e^\dagger_{\mathbf{k}-\mathbf{q}} e_{\mathbf{k}} + \frac{g_h(\mathbf{q})}{\sqrt{N}} h^\dagger_{\mathbf{k}-\mathbf{q}} h_{\mathbf{k}} \right] (b^\dagger_{\mathbf{q}} + b_{-\mathbf{q}}) - \sum_{\mathbf{pkk'}} \frac{U(\mathbf{p},\mathbf{k},\mathbf{k}')}{N}\, e^\dagger_{\mathbf{k}} h^\dagger_{\mathbf{p}-\mathbf{k}} h_{\mathbf{p}-\mathbf{k}'} e_{\mathbf{k}'}, \quad (1)$$

where $e^\dagger_{\mathbf{k}}$ [$h^\dagger_{\mathbf{k}}$] creates an electron [a hole] in the conduction [valence] band $\varepsilon_c(\mathbf{k})$ [$\varepsilon_v(\mathbf{k})$]. These electrons and holes feel an interband Coulomb attraction $U(\mathbf{p},\mathbf{k},\mathbf{k}')$ that may cause the formation of excitonic quasiparticles (electron-hole bound states) located in the gap between valence and conduction band. The coupling of the electrons [holes] to phonons created by $b^\dagger_{\mathbf{q}}$ is parametrized by $g_e(\mathbf{q})$ [$g_h(\mathbf{q})$], where $\omega_{\mathbf{q}}$ is the energy of lattice vibrations in the harmonic approximation ($\hbar = 1$). In Eq. (1), N is the number of lattice sites; $\mathbf{q}$, $\mathbf{p}$, $\mathbf{k}$, and $\mathbf{k}'$ are momenta.

In a simplified model, preserving essential features of the phenomenon, we consider two tight-binding bands of a simple cubic lattice,

$$\varepsilon_{c,v}(\mathbf{k}) = \hat{E}_{c,v} \pm (W_{c,v}/6) \sum_{\alpha=x,y,z} (1 - \cos k_\alpha), \qquad (2)$$

having bandwidths $W_{c,v}$, where the energy of the valence-band top is set to zero ($\hat{E}_v = 0$), i.e., the bottom of the conduction band gives the the direct band gap E_g at $\mathbf{k} = 0$, $\hat{E}_c = E_g$. Furthermore, we assume momentum independent Coulomb and electron-phonon interactions, $U(\mathbf{p},\mathbf{k},\mathbf{k}') \equiv U$, and $g_{e,h}(\mathbf{q}) \equiv g_{e,h}$, respectively, as well as dispersionless optical phonons $\omega_{\mathbf{q}} \equiv \Omega$. Then a dimensionless fermion-phonon coupling constant can be defined in the usual way as $\lambda_{e,h} = 2g^2_{e,h}/(W_{e,h}\Omega)$, and we consider the case $W_{c,v} = 3E_g$. The ground-state properties of the model (1) and (2) were previously analyzed [28].

B. Parameter regimes and material classes

Besides the ground state also the spectral properties of the exciton-polaron model (1) are determined by the complex interplay between (i) the Coulomb U/E_g attraction, (ii) the electron/hole-phonon coupling $\lambda_{e,h}$, and degree of adiabaticity. The latter reflects the retarded nature of the coupling of the fermions to the lattice vibrations and can be characterized by the following parameter ratios: (a1) Ω/E_g or $\Omega/W_{c,v}$ and (a2) Ω/E_b which basically place the the phonon frequency into relationship to one-particle (band gap or bandwidth) energies and many-particle (binding) energies, respectively. Thereby different material classes cover almost the whole range of physical parameters with respect to (i), (ii), (a1), and (a2), where small (large) ratios of (a1) and (a2) indicate an adiabatic (non-to-antiadiabatic) situation.

In several 3D materials a strong exciton-phonon interaction is realized. For example, the optical response of ZnO, having hexagonal wurtzite or cubic zinc-blende structure, exhibits a pronounced exciton (polaron) peak (pointing towards a binding energy of about 60 meV), which is accompanied by at least three sidebands related to a phonon frequency of about 70 meV [29–31]. Other examples are alkali halides [32] and thallous halides [33], where one can observe from three to five phonon sidebands. The alkali halides are clearly in the adiabatic regime with respect to (a2) because the typical binding energy of the exciton is about 1 eV [34,35], which is much larger than the frequencies of lattice vibrations (16–40 meV [32]) that participate in the exciton-polaron formation. On the other hand the binding energy of the exciton is about 12 (10) meV in the thallous halides TlCl (TlBr) and therefore are considerably smaller than the corresponding phonon frequency 22 (15) meV [33]. Hence, these materials are in the (a2) non-to-antiadiabatic regime. From this point of view, ZnO is in an intermediate adiabaticity regime because the exciton binding energy (∼60 meV) is comparable to the relevant phonon frequency (∼70 meV) [29–31].

We note that the ratio of the phonon frequency and the exciton binding energy of the exciton in a bulk material and its low-dimensional counterpart might differ. In a sense, this allows us tune the (a2) adiabaticity ratio by reducing the effective electronic dimensionality. Especially in monolayer systems the exciton binding energy can exceed those of the bulk system by an order of magnitude. Prominent examples are the transition-metal dichalcogenides WS_2 and WSe_2 with binding energies (phonon frequencies) ranging from 0.7 to 0.8 eV (30 to 100 meV) [36–38], whereas E_b of the bulk materials (∼55 meV) is comparable to the characteristic phonon frequencies. Another example is molybdenum disulfide MoS_2. Here the monolayer $E_b \simeq 400$ meV is considerably larger than the E_b bulk value of about 85 meV [39,40]. Since the phonon frequency in this material is in the order of 50 meV [39,40], monolayer and bulk systems typify different (a2) adiabaticity regimes.

Special caution is required when examining the (a1) adiabaticity in organic compounds. Here typical electronic bandwidths are in the range from 4 to 60 meV whereby the typical frequencies of intermolecular vibrations range from 3 to 25 meV [41–43]. Hence, the energy of the lattice vibrations can be either greater or less than the electronic bandwidth. In this regard, it has been known for a long time that manifestation of phonon sidebands strongly depends on the ratio between the electronic bandwidth and the phonon frequency [44]. Let us finally point out the rather exotic case of body-centered-orthorhombic sodium nitrite $NaNO_2$ which is in the profound nonadiabatic electron-phonon coupling regime: Here the phonon energy (∼12 meV) notably exceeds the exciton dispersion (∼0.4–0.6 meV) [45].

Analyzing in what follows the different parameter regimes (i), (ii), (a1), and (a2) for the 3D model (1), we can give an at least qualitatively correct picture of exciton-polaron formation also for electronically low-dimensional materials, simply by using the corresponding parameter ratios. This is also supported by the experimental indications that the decisive control parameter for exciton-polaron formation is mainly the ratio between electronic and phononic energy scales and not so much the effective spatial dimensionality of the problem [44].

III. ABSORPTION SPECTRA AT PARTICULAR PHYSICAL REGIMES

Discussing the optical properties of exciton polarons, we look at the photon-absorption transition rate, which is proportional to the spectral function $A(\omega)$ that itself is related to the real part of the optical conductivity $\sigma(\omega)$ by

$$\mathrm{Re}[\sigma(\omega)] = A(\omega)/\omega,$$

Ref. [46]. To figure out polaronic effects, we impose the normalization $\int_0^\infty d\omega A(\omega) = 1$. In order to disentangle to some extent the complex interplay between Coulomb and electron/hole-phonon-coupling effects in the process

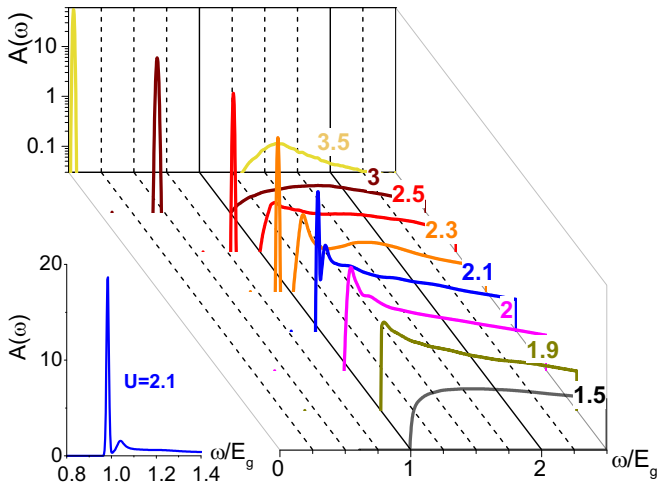

FIG. 1. Spectral function $A(\omega)$ for the pure excitonic model ($\lambda_e = \lambda_h = 0$) at different U/E_g. Inset in the left shows $A(\omega)$ at $U/E_g = 2.1$ in linear scale.

of (exciton-polaron) bound-state formation, we analyze in what follows different characteristic situations for the three-dimensional case.

A. Pure Coulomb attraction

Our starting point is the optical response of the Coulomb-only interacting electron-hole system. From Fig. 1 one clearly sees (i) the optical-absorption threshold $\omega \simeq E_g$ for small U/E_g, (ii) how spectral weight accumulates at the bottom of the optical spectra as U/E_g increases, (iii) that an excitonic peak splits off at the critical value $U_c/E_g \simeq 1.98$, which (iv) separates more and more from the broad absorption band until it requires zero excitation energy for very large Coulomb attractions when the exciton level approaches the valence-band top.

B. Coupling to the lattice: Adiabatic case

Here we first neglect the Coulomb interaction between electrons and holes ($U = 0$). Results are inserted in Fig. 2(a). Working in the (a1) adiabatic regime, we observe (i) the lowering of the optical-absorption threshold as the fermion-phonon coupling $g_e = g_h$ increases and (ii), at larger values of λ, an undulated absorption signal related to multi-phonon-involved processes when polaron formation sets in. Adding the coupling to the lattice degrees of freedom to the Coulomb attraction, in comparison to Fig. 1, electron-hole bound states develop at substantially lower values of U [note that $U < U_c$ in Fig. 2(b)]. Now the quasiparticle formed is largely dressed by phonons however, and therefore can be viewed as an exciton polaron. The polaron exciton is characterized by a low spectral weight of the electronic part of the optical response because the electron-hole bound state is entangled with a many-phonon (cloud) state. Then the small low-energy peak at $\lambda = 0.18$ in Fig. 2(b), separated from the rest of the spectra, is what is left projecting the exciton-polaron signal to a zero-phonon state. In accordance with that, the preexisting strong excitonic peak drawn for $U/E_g = 3$ and $\lambda = 0$ [see Fig. 2(c)] is not only shifted to lower energies but lowered in intensity when

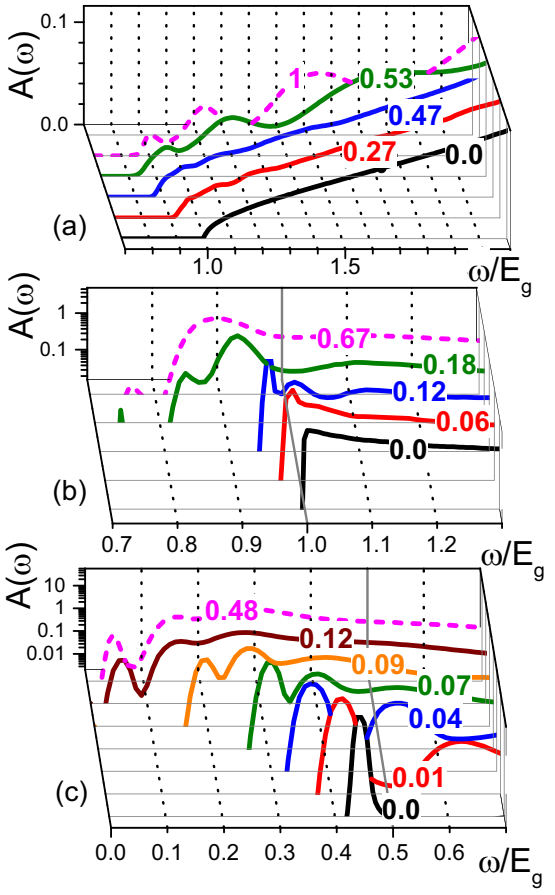

FIG. 2. Optical response depending on the fermion-phonon interaction strength (given at spectra) in the adiabatic regime $\Omega/E_g = 0.1$, where $U = 0$ (a), $U/E_g = 1.9$ (b), and $U/E_g = 3.0$ (c). Results for $\lambda_e = \lambda_h$ are given by solid lines; dashed magenta lines indicate the typical behavior when $\lambda_e > 0$ and $\lambda_h = 0$.

the fermion-phonon coupling comes in to play. Intensity of low-energy peaks in Figs. 2(b) and 2(c) is lost to a series of phonon sidebands higher in energy, separated by the phonon frequency $\Omega = 0.1E_g$. This can be taken as a signature for exciton-polaron formation due to the constructive interplay of Coulomb and fermion-phonon interaction. Hence notable polaronic effects are observed even in the weak fermion-phonon coupling regime. We exemplarily included in Fig. 2 the case where the coupling to phonons takes place in the conduction band only (see dashed lines). Despite that the fermion-phonon interaction has to be approximately twice (four times) as large to form exciton polarons for $U = 0$ ($U \simeq U_c$), i.e., when a conduction-band polaron catches the hole in the valence band developing a bound state, the spectra do not change much qualitatively.

Let us emphasize that the pattern of phonon sidebands appearing in Fig. 2 is observed in the optical spectra in a whole range of different materials; see, e.g., Refs. [22,44,47–49]. Note that the pattern of the phonon sidebands in the (a1) adiabatic regime strongly depends on the (a2) adiabaticity parameter Ω/E_b. In the case of (a2) nonadiabaticity $\Omega/E_b > 1$ [see Fig. 2(b) for $\lambda = 0.06$ and $\lambda = 0.12$], the energy separation of the first phonon sideband from the main exciton peak is

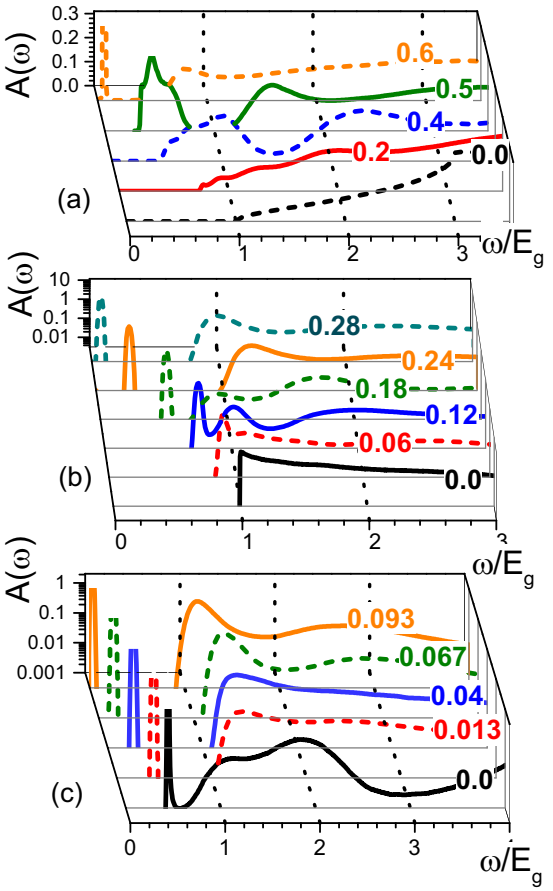

FIG. 3. Spectral function $A(\omega)$ in the nonadiabatic regime $\Omega/E_g = 1$ at various $\lambda = \lambda_{e,h}$ (given at spectra) for (a) $U = 0$, (b) $U/E_g = 1.9$, and (c) $U/E_g = 3.0$.

less than Ω whereas the distance between the higher sidebands corresponds more or less exactly with Ω. This is in accordance with the experimental data for MgO, BeO, TlCl, and TlBr which are in the (a2) nonadiabatic regime [33,50–54]. On the other hand, all sidebands are separated by Ω when $\Omega/E_b \leqslant 1$; see Figs. 2(c) and 2(b) for $\lambda = 0.18$. This is in agreement with the experimental data on (a2)-type adiabatic exciton polarons in alkali halides [32,34,35], as well as for the intermediate case—regarding the adiabaticity ratio—of ZnO [29–31].

C. Coupling to the lattice: Nonadiabatic case

Let us now take a closer look at the (a1) antiadiabatic regime. Figure 3 presents the optical response for $\Omega/E_g = 1$, i.e., the energy for bridging the band gap by photon absorption is the same as exciting one phonon. Recall that the polaron crossover is much smoother in the (a1) antiadiabatic regime than in the adiabatic one, and a stronger fermion-phonon coupling $g_{e,h}$ is necessary because now the ratio between the polaron binding energy and the large frequency of the phonons matters [55,56]. Large Ω is reflected in Fig. 3(a) for $U = 0$ in modulation of the spectral weight at the large phonon scale ($\Omega = 1$). Due to resonance $\Omega = E_g$ condition the low-energy peak, which can be attributed to an "bipolaronic" (electron-hole) quasiparticle bound by fermion-phonon interaction only [28,57], becomes separated from the rest of the spectrum not at $\lambda = 0.5$, as predicted in [28,57], but only when $\lambda = 0.6$. For $\lambda = 0.5$, the lowest bump consists of three overlapping absorption signatures, separated by energies less than the phonon frequency. This is because calculating $A(\omega)$ we have to integrate over the momenta and, in the transition region, the bipolaron splits off from two (conduction and valence) bands having a renormalized (but still finite) bandwidth each, which leads to a central peak and a lower (upper) satellites when the bipolaron band develops. By contrast, when the fermion-phonon interaction is present in only one of bands, we observed only a two-peak structure in the crossover regime (not shown). Figures 3(b) and 3(c) with $U/E_g = 1.9$ and $U/E_g = 3.0$, respectively, illustrate the development of exciton polarons in the (a1) antiadiabatic regime. Here the fermion-phonon coupling λ again triggers the formation of a bound state for $U < U_c$ [see the curves for $\lambda = 0.18$, 0.24, and 0.28 in (b)], and a notable shift of the excitonic level towards the top of the valence band for $U > U_c$ [compare, in particular, Figs. 1 and 3(c)]. A similar scenario is observed when only the electrons in the conduction band couple to phonons whereby, in this case, a larger (one-band) electron-phonon interaction is necessary.

Obviously, the dependence of the sideband pattern on the (a2) adiabatic parameter Ω/E_b is now very similar in both the (a1) adiabatic and (a1) nonadiabatic regimes. Thereby the separation of the first phonon sideband from the main exciton peak is less than the phonon energy Ω in the case of (a2) nonadiabaticity, whereas it is approximately equal to Ω when $\Omega/E_b \leqslant 1$. This trend can be clearly seen in the evolution of the absorption spectra when going from $\lambda = 0.06$ to 0.28 in Fig. 3(b), and going from $\lambda = 0.013$ to 0.093 in Fig. 3(c). The conclusive role of the (a2) adiabaticity parameter Ω/E_b is confirmed by experiments on the "nonadiabatic" MgO, BeO, TlCl, and TlBr [33,50–54] compounds, the "adiabatic" alkali halides [32,34,35], and the "intermediate" case of ZnO [29–31].

IV. DIAGRAMMATICS FOR THE CURRENT-CURRENT CORRELATION FUNCTION

The spectral function $A(\omega)$ is obtained by analytic continuation of the imaginary time current-current correlation function $\Pi(\tau) = \langle \text{vac}|T_\tau \mathbf{j}(\tau)\mathbf{j}(0)|\text{vac}\rangle$ to real frequencies, solving the equation $\Pi(\tau) = \int_0^\infty d\omega \exp(-\tau\omega)A(\omega)$ by the stochastic optimization consistent constraint method [26,58–60]. The current operator, in real space, is defined as $\mathbf{j} = i[H, \mathbf{P}]$ with the polarization operator $\mathbf{P} = -e\mathbf{D}\sum_j e_j^\dagger h_j^\dagger + \text{H.c.}$, where $\mathbf{D} = \int d\mathbf{r}\phi_e^*(\mathbf{r})\mathbf{r}\phi_h(\mathbf{r})$ is the interband electron-hole dipole matrix element [46]. For the model (1) and (2) under study, we obtain (e.g., in the x direction): $j_x = j_x^{(f)} + j_x^{(p)}$, i.e., a sum of a purely fermionic contribution,

$$j_x^{(f)} = ieD_x \sum_{\mathbf{k}} f(\mathbf{k}) X_{\mathbf{k}} + \text{H.c.}, \tag{3}$$

and a polaronic contribution,

$$j_x^{(p)} = \frac{ieD_x}{\sqrt{N}}(g_e + g_h) \sum_{\mathbf{kq}} Y_{\mathbf{k},\mathbf{q}} + \text{H.c.}, \tag{4}$$

where $X_{\mathbf{k}} = c_{\mathbf{k}}^\dagger h_{-\mathbf{k}}^\dagger$, $Y_{\mathbf{k},\mathbf{q}} = c_{\mathbf{k}}^\dagger h_{-\mathbf{k}-\mathbf{q}}^\dagger (b_{\mathbf{q}}^\dagger + b_{-\mathbf{q}})$, and $f(\mathbf{k}) = -(W_c + W_v)/6 \sum_\alpha [1 - \cos(k_\alpha)] - E_g + U$. For the limiting

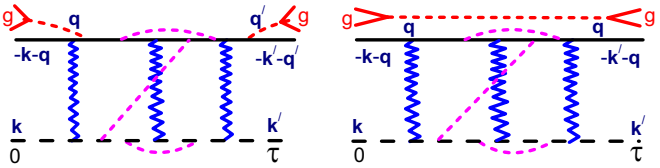

FIG. 4. Typical diagrams in the Feynman expansion of the current-current correlations function. Here solid (dashed) horizontal black lines represent electron (hole) propagators, dotted magenta lines denote phonon propagators, and wiggled blue lines symbolize the Coulomb attraction between electrons and holes. According to the absence (presence) of zero, one, or two phonon propagators attached at imaginary times 0 or τ (red dotted line marked by "g"), we obtain four different topologies of the left diagram. Presence (absence) of g propagator means that the correlation function is terminated by the operator $X_{\mathbf{k}}$ ($Y_{\mathbf{k},\mathbf{q}}$).

case of a wide-gap semiconductor ($E_g \to \infty$) $f(\mathbf{k}) = f_c$ is a constant whose absolute value $|f_c|$ is larger than all other characteristic energies W_c, W_v, and the maximum $\omega_{\mathbf{q}}$. The detailed functional form of $f(\mathbf{k})$ only marginally affects the results for the spectral function and $f(\mathbf{k}) = f_c$ is set to unity (as well as electron charge, matrix element $|D_x|$, and Planck constant $\hbar$) for the calculations presented above. Also, we will first neglect the polaronic contribution to the current and discuss its influence separately below.

Adapting the DMC method to the calculation of the optical spectrum $A(\omega)$, we rewrite the current-current correlation function in interaction representation and expand it with respect to both Coulomb attraction (U) and fermion-phonon coupling ($g_{e,h}$) strengths. Typical phonon-dressed ladder-type Feynman diagrams [61], which contribute in such a series expansion, are depicted in Fig. 4. The weight attributed to a given diagram is the product of the interaction vertices [$U(\mathbf{p},\mathbf{k},\mathbf{k}')$, $g_e(\mathbf{q})$, and $g_h(\mathbf{q})$] and Matsubara Green functions (for electrons, holes, and phonons) at imaginary times (τ), where momentum conservation is imposed by the Hamiltonian (1). We point out that the DMC updates of Coulomb vertices and phonon propagators are similar to those used for the pure exciton [27,28] and polaron [26] problem, respectively. The main difference between the previous and present DMC implementations is due to the two distinct current operator contributions, (3) and (4). Accordingly, the DMC now has to switch between four topological different classes of Feynman diagrams, namely XX, XY, YX, and YY, depending on whether the beginning or end of the current-current correlation function is terminated by X or Y operators; see Fig. 4. The new DMC approach was validated, for the one-dimensional case, using expressions (3) and (4), by comparison with a truncated phonon-space exact diagonalization of (1) [62–64]. We work within DMC in the thermodynamic limit $N \to \infty$.

Figure 5 illustrates the influence and relative importance of the electron $\mathbf{j}^{(f)}$ and polaron $\mathbf{j}^{(p)}$ parts of the current to the spectral function $A(\omega)$. In the adiabatic regime, the polaronic current significantly contributes to the low-energy optical response of the system but the peak positions and the overall line shape are unaltered. By contrast, in the antiadiabatic regime, the lowest peak, attributed to exciton polarons, is less affected by $\mathbf{j}^{(p)}$ regarding the spectral weight; now $\mathbf{j}^{(p)}$ primarily influences the threshold and shape of the upper absorption band.

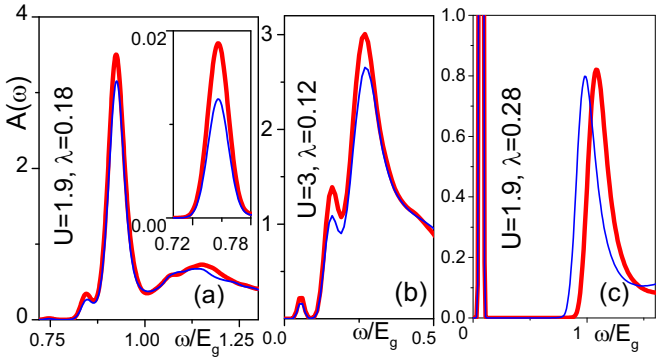

FIG. 5. Contributions to the optical response, $A(\omega)$, in the adiabatic $\Omega/E_g = 0.1$ [(a) and (b)] and antiadiabatic $\Omega/E_g = 1.0$ (c) cases. The fermion-phonon couplings are assumed to be the same in the valence and conduction bands, $\lambda_{e,h} = \lambda$. Thick red (thin blue) lines give results when both current contributions $\mathbf{j}^{(f)}$ and $\mathbf{j}^{(p)}$ (only $\mathbf{j}^{(f)}$) were included.

V. CONCLUSIONS

To sum up, utilizing a refined diagrammatic Monte Carlo method, we discussed the optical absorption of photons by exciton polarons within a paradigmatic two-band model, treating Coulomb and fermion-phonon coupling effects on an equal footing. The results are unbiased, and were derived for the infinite system in three dimensions. Even though both interactions promote the formation of electron-hole bound states in the band gap, the resulting quasiparticles—and consequently their optical signatures—can be very different depending on the relative strength of the Coulomb attraction and the coupling to the lattice degrees of freedom where also retardation effects play an important role. While the predominantly Coulomb-bound exciton polaron shows a strong and narrow resonance, the optical signal of an exciton heavily dressed by phonons has a much lower spectral weight, similar to bipolarons. When the phonons are slow (adiabatic regime), the low-energy contribution resulting from the polaronic part of the current-current correlation function is substantial, whereas for fast phonons, in the non-to-antiadiabatic regime, the polaronic current mainly affects the threshold and line shape of the upper optical-absorption band. We furthermore show that the distance of the first phonon sideband from the zero phonon line is smaller than the separation of the consequent higher energy sidebands when the phonon frequency is larger than the exciton binding energy. In this way our model calculations will support the analysis of optical-absorption measurements in a wide class of correlated materials.

ACKNOWLEDGMENT

This work was supported by the ImPACT Program of the Council for Science, Technology and Innovation (Cabinet Office, Government of Japan), and by the Deutsche Forschungsgemeinschaft through SFB 652.

[1] *Handbook of Spectroscopy*, edited by G. Gauglitz and T. Vo-Dinh (Wiley-VCH Verlag GmbH, Weinheim, 2003), Vols. 1 and 2, 1168 pp.

[2] Y. Toyozawa, *Optical Processes in Solids* (Cambridge University Press, Cambridge, UK, 2003).

[3] I. Egri, Phys. Rep. **119**, 363 (1985).

[4] M. Ueta, H. Kanzaki, K. Kobayashi, Y. Toyozawa, and E. Hanamura, *Excitonic Processes in Solids* (Springer-Verlag, Berlin, 1986).

[5] *Polarons and Excitons in Polar Semiconductors and Ionic Crystals*, edited by J. T. Devreese and F. M. Peeters (Plenum, New York, 1984).

[6] *Excitonic Processes in Condensed Matter*, edited by R. T. Williams and W. M. Yen (Electrochemical Society, Pennington, NJ, 1998).

[7] *Optical Properties of Low-dimensional Materials*, edited by T. Ogawa and Y. Kanemitsu (World Scientific, Singapore, 1998), Vol. 2.

[8] J. Bardeen and W. Shockley, Phys. Rev. **80**, 72 (1950).

[9] M. V. Fischetti and S. E. Laux, J. Appl. Phys. **80**, 2234 (1996).

[10] S.-H. Wei and A. Zunger, Phys. Rev. B **60**, 5404 (1999).

[11] V. M. Fomin, V. N. Gladilin, J. T. Devreese, E. P. Pokatilov, S. N. Balaban, and S. N. Klimin, Phys. Rev. B **57**, 2415 (1998).

[12] O. Verzelen, R. Ferreira, and G. Bastard, Phys. Rev. Lett. **88**, 146803 (2002).

[13] E. G. Wilson, J. Phys. C: Solid State Phys. **16**, 1039 (1983).

[14] B. I. Halperin and T. M. Rice, Rev. Mod. Phys. **40**, 755 (1968).

[15] V.-N. Phan, K. W. Becker, and H. Fehske, Phys. Rev. B **88**, 205123 (2013).

[16] B. Zenker, H. Fehske, and H. Beck, Phys. Rev. B **90**, 195118 (2014).

[17] B. Zenker, H. Fehske, H. Beck, C. Monney, and A. R. Bishop, Phys. Rev. B **88**, 075138 (2013).

[18] T. Kaneko, T. Toriyama, T. Konishi, and Y. Ohta, Phys. Rev. B **87**, 035121 (2013).

[19] T. E. Kidd, T. Miller, M. Y. Chou, and T. C. Chiang, Phys. Rev. Lett. **88**, 226402 (2002).

[20] P. Wachter, B. Bucher, and J. Malar, Phys. Rev. B **69**, 094502 (2004).

[21] P. Wachter and B. Bucher, Physica B **408**, 51 (2013).

[22] A. S. Mishchenko and N. Nagaosa, Phys. Rev. Lett. **86**, 4624 (2001).

[23] A. S. Mishchenko, N. Nagaosa, N. V. Prokof'ev, A. Sakamoto, and B. V. Svistunov, Phys. Rev. B **66**, 020301(R) (2002).

[24] A. Sumi, J. Phys. Soc. Jpn. **43**, 1286 (1977).

[25] N. V. Prokof'ev and B. V. Svistunov, Phys. Rev. Lett. **81**, 2514 (1998).

[26] A. S. Mishchenko, N. V. Prokof'ev, A. Sakamoto, and B. V. Svistunov, Phys. Rev. B **62**, 6317 (2000)

[27] E. A. Burovski, A. S. Mishchenko, N. V. Prokof'ev, and B. V. Svistunov, Phys. Rev. Lett. **87**, 186402 (2001).

[28] E. Burovski, H. Fehske, and A. S. Mishchenko, Phys. Rev. Lett. **101**, 116403 (2008).

[29] H. Sezen, H. Shang, F. Bebensee, C. Yang, M. Buchholz, A. Nefedov, S. Heissler, C. Carbogno, M. Scheffler, P. Rinke, and C. Woll, Nat. Commun. **6**, 6901 (2015).

[30] S. J. Xu, S.-J. Xiong, and S. L. Shi, J. Chem. Phys. **123**, 221105 (2005).

[31] J. A. Sans, A. Segura, M. Mollar, and B. Mari, Thin Solid Films **453–454**, 251 (2004).

[32] G. Baldini, A. Bosacchi, and B. Bosacchi, Phys. Rev. Lett. **23**, 846 (1969).

[33] S. Kurita and K. Kobayashi, J. Phys. Soc. Jpn. **30**, 1645 (1971).

[34] T. Nakayama, J. Phys. Soc. Jpn. **65**, 2188 (1996).

[35] R. Webster, L. Bernasconi, and N. M. Harrison, J. Chem. Phys. **142**, 214705 (2015).

[36] A. T. Hanbicki, M. Currie, G. Kioseoglou, A. L. Friedman, and B. T. Jonker, Solid State Commun. **203**, 16 (2015).

[37] C. M. Chow, H. Yu, A. M. Jones, J. Yan, D. G. Mandrus, T. Taniguchi, K. Watanabe, W. Yao, and X. Xu, Nano Lett. **17**, 1194 (2017).

[38] B. Zhu, X. Chen, and X. Cui, Sci. Rep. **5**, 9218 (2015).

[39] N. Saigal, V. Sugunakar, and S. Ghosh, Appl. Phys. Lett. **108**, 132105 (2016).

[40] B. R. Carvalho, L. M. Malard, J. M. Alves, C. Fantini, and M. A. Pimenta, Phys. Rev. Lett. **114**, 136403 (2015).

[41] H. Sumi, J. Chem. Phys. **67**, 2943 (1977).

[42] A. Matsui, K. Tomioka, Y. Oeda, and T. Tomotika, Surf. Sci. **37**, 849 (1973).

[43] S. D. Colson, D. M. Hanson, R. Kopelman, and G. W. Robinson, J. Chem. Phys. **48**, 2215 (1968).

[44] R. M. Hochstrasser and P. N. Prasad, J. Chem. Phys. **56**, 2814 (1972).

[45] M. Ashida, Y. Kawaguchi, and R. Kato, J. Phys. Soc. Jpn. **58**, 4620 (1989).

[46] G. D. Mahan, *Many Particle Physics* (Plenum, New York, 1990).

[47] S. J. Xu, G. Q. Li, S.-J. Xiong, S. Y. Tong, C. M. Che, W. Liu, and M. F. Li, J. Chem. Phys. **122**, 244712 (2005).

[48] S. J. Xu, G. Q. Li, S.-J. Xiong, and C. M. Che, J. Appl. Phys. **99**, 073508 (2006)

[49] A. Brillante and M. R. Philpott, J. Chem. Phys. **72**, 4019 (1980).

[50] W. Y. Liang and A. D. Yoffe, Phys. Rev. Lett. **20**, 59 (1968).

[51] R. C. Whited and W. C. Walker, Phys. Rev. Lett. **22**, 1428 (1969).

[52] W. C. Walker, D. M. Roessler, and E. Loh, Phys. Rev. Lett. **20**, 847 (1968).

[53] R. Z. Bachrach and F. C. Brown, Phys. Rev. Lett. **21**, 685 (1968).

[54] R. Z. Bachrach and F. C. Brown, Phys. Rev. B **1**, 818 (1970).

[55] G. Wellein and H. Fehske, Phys. Rev. B **58**, 6208 (1998).

[56] A. Alvermann, H. Fehske, and S. A. Trugman, Phys. Rev. B **81**, 165113 (2010).

[57] A. Macridin, G. A. Sawatzky, and M. Jarrell, Phys. Rev. B **69**, 245111 (2004).

[58] A. S. Mishchenko, in *Correlated Electrons: From Models to Materials Modeling and Simulation*, edited by E. Pavarini, E. Koch, F. Anders, and M. Jarrell (Verlag des Forschungszentrum, Jülich, 2012), Vol. 2.

[59] N. V. Prokof'ev and B. V. Svistunov, JETP Lett. **97**, 649 (2013).

[60] O. Goulko, A. S. Mishchenko, L. Pollet, N. Prokof'ev, and B. Svistunov, Phys. Rev. B **95**, 014102 (2017).

[61] A. L. Fetter and J. D. Walecka, *Quantum Theory of Many-particle Systems* (McGraw-Hill, New York, 1971).

[62] G. De Filippis, V. Cataudella, A. S. Mishchenko, and N. Nagaosa, Phys. Rev. B **85**, 094302 (2012).

[63] D. J. J. Marchand, G. De Filippis, V. Cataudella, M. Berciu, N. Nagaosa, N. V. Prokof'ev, A. S. Mishchenko, and P. C. E. Stamp, Phys. Rev. Lett. **105**, 266605 (2010).

[64] G. De Filippis, V. Cataudella, E. A. Nowadnick, T. P. Devereaux, A. S. Mishchenko, and N. Nagaosa, Phys. Rev. Lett. **109**, 176402 (2012).